J|A|C|S ARTICLES

Published on Web 09/14/2010

Multistimuli Two-Color Luminescence Switching via Different Slip-Stacking of Highly Fluorescent Molecular Sheets

Seong-Jun Yoon,[†] Jong Won Chung,[†] Johannes Gierschner,*[,‡] Kil Suk Kim,[§] Moon-Gun Choi,[||] Dongho Kim,*[,§] and Soo Young Park*[,†]

Center for Supramolecular Optoelectronic Materials and WCU Hybrid Materials Program, Department of Materials Science and Engineering, Seoul National University, ENG 445, Seoul 151-744, Korea, Madrid Institute for Advanced Studies, IMDEA Nanoscience, UAM, Modulo C-IX, AV. Tomás y Valiente 7, Campus de Cantoblanco, 28049 Madrid, Spain, Spectroscopy Laboratory for Functional π-Electronic Systems and Department of Chemistry, Yonsei University, Seoul 120-749, Korea, and Department of Chemistry and Center for Bioactive Molecular Hybrids, Yonsei University, Seoul 120-749, Korea

Received November 11, 2009; E-mail: parksy@snu.ac.kr (S.Y.P.); johannes.gierschner@imdea.org (J.G.); dongho@yonsei.ac.kr (D.K.)

Abstract: Color tuning and switching of the solid-state luminescence of organic materials are attractive subjects for both the fundamental research and practical applications such as optical recording. We report herein cyanostilbene-based highly luminescent molecular sheets which exhibit two-color fluorescence switching in response to pressure, temperature, and solvent vapor. The origin for the multistimuli luminescence switching is the two-directional shear-sliding capability of molecular sheets, which are formed via intermolecular multiple C−H···N and C−H···O hydrogen bonds. The resulting two distinctive crystal phases are promoted by different modes of local dipole coupling, which cause a substantial alternation of π−π overlap. These changes can be directly correlated with the subsequent intermolecular excitonic and excimeric coupling in both phases, as demonstrated by an in-depth theory-assisted spectroscopic and structural study. Finally, we have prepared a first device demonstrator for rewritable fluorescent optical recording media which showed multistimuli luminescence tuning with fast response. Our multistimuli responsive system is unique in terms of the slip-stacking of molecular sheets and thus provides a novel concept of rewritable fluorescent optical recording media.

1. Introduction

In the past years, much attention has been paid on aggregation phenomena of conjugated organic materials particularly related to their applications in (opto-)electronic devices.[1] To establish meaningful structure−property relationships in the solid state, the subtle interplay of molecular and supramolecular level structures and the envisaged properties has to be understood.[2,3] Tuning solid-state properties, in particular (dynamic) solid-state fluorescence switching, with high efficiency and reproducibility by controlling the molecular stacking without changing the chemical structure of the constituting molecules not only provides fundamental understanding but also has practical application in optical recording and sensing. Various examples of fluorescence color change driven by molecular aggregation and/or stacking have been reported,[4−9] although the in-depth theoretical understanding of the phenomena has rather been limited.

Within this line of idea, cyano stilbene derivatives have been investigated in recent years,[10,11] where the extremely large fluorescence enhancement in the solid state (nanoparticle, powder, gel, etc.) was attributed not only to the spatial confinement effect but also to the formation of specific supramolecular stacking architecture associated with the unique electronic and geometrical characteristics of the designed molecules. This cooperative behavior, commonly known as aggregation-induced enhanced emission (AIEE),[10] is of great practical importance because of its solid-state applications, particularly in (opto-)electronic devices. Moreover, highly fluorescent materials in the solid state are expected to offer solid-state luminescence switching when incorporated with stimuli-responsive units. We have recently demonstrated various stimuli-responsive AIEE systems, such as fluorescent photochromic

[†] Seoul National University.
[‡] Madrid Institute for Advanced Studies, IMDEA Nanoscience, UAM.
[§] Spectroscopy Laboratory for Functional π-Electronic Systems and Department of Chemistry, Yonsei University.
[||] Department of Chemistry and Center for Bioactive Molecular Hybrids, Yonsei University.

(1) Hoeben, F. J. M.; Jonkheijm, P.; Meijer, E. W.; Schenning, A. P. H. J. *Chem. Rev.* **2005**, *105*, 1491.
(2) Gierschner, J.; Ehni, M.; Egelhaaf, H. J.; Milián Medina, B.; Beljonne, D.; Benmansour, H.; Bazan, G. C. *J. Chem. Phys.* **2005**, *123*, 144914.
(3) (a) Curtis, M. D.; Cao, J.; Kampf, J. W. *J. Am. Chem. Soc.* **2004**, *126*, 4318. (b) Dong, J.; Solntsev, K. M.; Tolbert, L. M. *J. Am. Chem. Soc.* **2009**, *131*, 662.
(4) (a) Brinkmann, M.; Gadret, G.; Muccini, M.; Taliani, C.; Masciocchi, N.; Sironi, A. *J. Am. Chem. Soc.* **2000**, *122*, 5147. (b) Sanz, N.; Baldeck, P. L.; Nicoud, J. F.; Fur, Y. L.; Ibanez, A. *Solid State Sci.* **2001**, *3*, 867. (c) Gierschner, J.; Egelhaaf, H. J.; Mack, H. J.; Oelkrug, D.; Martinez Alvarez, R.; Hanack, M. *Synth. Met.* **2003**, *137*, 1449. (d) Schweikhart, K. H.; Hohloch, M.; Steinhuber, E.; Hanack, M.; Lüer, L.; Gierschner, J.; Egelhaaf, H. J.; Oelkrug, D. *Synth. Met.* **2001**, *121*, 1641.

nanoparticles and polymer films,[12] highly sensitive fluorescence probes for organic vapors,[13] array patterning of fluorescent nanoparticles,[14] fluorescent switchable smart gels,[15] and fluorescent switchable π-dimer crystals,[9e] which respond to various external stimuli including light, organic vapor, acid, temperature, and pressure. Meanwhile, some cyano distyrylbenzene (DSB) derivatives have also been shown to exhibit reversible piezochromism by C. Weder group.[8c]

Herein, we have synthesized a new AIEE-active cyano DSB derivative, (2*Z*,2′*Z*)-2,2′-(1,4-phenylene)bis(3-(4-butoxyphenyl) acrylonitrile), DBDCS (see Scheme 1). DBDCS exhibits very high solid-state fluorescence quantum yield (62%) due to the characteristic AIEE process, as well as multistimuli two-color luminescence switching. DBDCS uniquely forms fluorescent 'molecular sheets' with stacking and shear-sliding capabilities, which are responsible for stimuli-responsive luminescence switching behavior.

Scheme 1. Molecular Structure of DBDCS and Its Local Dipoles (dashed arrows) and Transition Dipole Moment $\mu(S_0 \rightarrow S_1)$ (double arrow, the length of 12.6 D) and Dihedral Torsional Angles in Isolated State and Single Crystal State (in brackets)

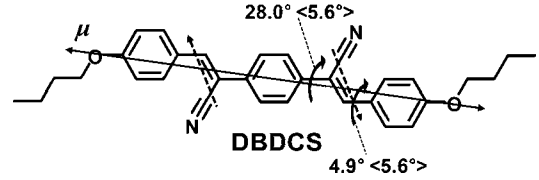

We have utilized this phenomenon to successfully develop rewritable fluorescent optical recording media which showed fast-responding multistimuli luminescence switching. This multistimuli responsive system may find practical applications in optical memory systems. Furthermore, it offers an intriguing example how to understand and utilize structure−property relationships in the solid-state fluorescence emission behavior. To gain further insight into this phenomenon, we have comprehensively explored the structural, optical and photophysical properties, assisted by quantum-chemical calculations.

2. Experimental and Computational Methods

2.1. Synthesis and Characterization. (2*Z*,2′*Z*)-2,2′-(1,4-phenylene)bis(3-(4-butoxyphenyl) acrylonitrile), DBDCS (see Scheme 1), was synthesized via Knoevenagel reaction of 4-butoxy-benzaldehyde and (4-cyanomethyl-phenyl)-acetonitrile. Full synthetic details, ^{1}H NMR, ^{13}C NMR, mass spectroscopy, and elemental analysis characterization are found in the Supporting Information (SI).

2.2. Sample Preparation. Nanoparticle suspensions were obtained by a simple reprecipitation method from DBDCS solution in THF (2×10^{-5} mol L^{-1}) by injection of water (distilled and filtered by membrane filter with 0.2 μm pore size) in 1:4 volume fraction under vigorous stirring.[16] Single crystals were obtained from the ethyl acetate solution at room temperature. Powder samples were prepared by recrystallization from hot ethanol solutions as pale whitish sheet-like crystallites. Thin films (thickness of 50 nm) were fabricated on quartz substrates by vacuum deposition.

2.3. X-ray and Thermal Analysis. A single crystal was selected under ambient condition, coated in epoxy, and mounted on the end of a glass fiber. Crystal data collection was performed on a Bruker CCD Apex diffractometer with Mo Kα ($\lambda = 0.71073$ Å) radiation and a collector-to-crystal distance of 5.99 cm. Cell constants were determined from a list of reflections found by an automated search routine. Data were collected using the full sphere routine and corrected for Lorentz and polarization effects. The absorption corrections were based on fitting a function to the empirical transmission surface as sampled by multiple equivalent measurements using SADABS software. SAXS measurements were performed on a GADDS (Bruker, Germany) equipped with a 2D area detector, operating at 3 kW. XRD measurements were performed on a Powder X-ray Diffractometry (Bruker, Germany), operating at 3 kW. Differential scanning calorimetry (DSC) was performed on a Perkin-Elmer DSC7 at a heating rate of 5 °C min^{-1}.

2.4. Spectroscopic Characterization. ^{1}H NMR spectra were recorded on a JEOL JNM-LA300 (300 MHz) in $CDCl_3$ solutions. Mass spectra were measured using a JEOL, JMS AX505WA mass spectrometer. Elemental analysis was carried out using a CE instruments EA1110 elemental analyzer. FE-SEM images were acquired on a JSM-6330F (JEOL). UV−visible absorption spectra

(5) (a) Davis, R.; Rath, N. P.; Das, S. *Chem. Commun.* **2004**, 74. (b) Mutai, T.; Satou, H.; Araki, K. *Nat. Mater.* **2005**, *4*, 685. (c) Zhang, H.; Zhang, Z.; Ye, K.; Zhang, J.; Wang, Y. *Adv. Mater.* **2006**, *18*, 2369. (d) Mutai, T.; Tomoda, H.; Ohkawa, T.; Yabe, Y.; Araki, K. *Angew. Chem., Int. Ed.* **2008**, *47*, 9522. (e) Zhao, Y.; Gao, H.; Fan, Y.; Zhou, T.; Su, Z.; Liu, Y.; Wang, Y. *Adv. Mater.* **2009**, *21*, 3165.

(6) (a) Davis, R.; Kumar, N. S. S.; Abraham, S.; Suresh, C. H.; Rath, N. P.; Tamaoki, N.; Das, S. *J. Phys. Chem. C* **2008**, *112*, 2137. (b) Kumar, N. S. S.; Varghese, S.; Rath, N. P.; Das, S. *J. Phys. Chem. C* **2008**, *112*, 8429. (c) Thomas, R.; Varghese, S.; Kulkarni, G. U. *J. Mater. Chem.* **2009**, *19*, 4401. (d) Kumar, N. S. S.; Varghese, S.; Suresh, C. H.; Rath, N. P.; Das, S. *J. Phys. Chem. C* **2009**, *113*, 11927. (e) Zhang, Z.; Zhang, Y.; Yao, D.; Bi, H.; Javed, I.; Fan, Y.; Zhang, H.; Wang, Y. *Cryst. Growth Des.* **2009**, *9*, 5069.

(7) (a) Kishimura, A.; Yamashita, T.; Yamaguchi, K.; Aida, T. *Nat. Mater.* **2005**, *4*, 546. (b) Dong, Y.; Lam, J. W. Y.; Qin, A.; Li, Z.; Sun, J.; Sung, H. H. Y.; Williams, I. D.; Tang, B. Z. *Chem. Commun.* **2007**, 40. (c) Dong, Y.; Lam, J. W. Y.; Qin, A.; Sun, J.; Liu, J.; Li, Z.; Sun, J.; Sung, H. H. Y.; Williams, I. D.; Kwok, H. S.; Tang, B. Z. *Chem. Commun.* **2007**, 3255. (d) Srinivasan, S.; Babu, P. A.; Mahesh, S.; Ajayaghosh, A. *J. Am. Chem. Soc.* **2009**, *131*, 15122.

(8) (a) Gawinecki, R.; Viscardi, G.; Barni, E.; Hanna, M. A. *Dyes Pigments* **1993**, *23*, 73. (b) Sagara, Y.; Mutai, T.; Yoshikawa, I.; Araki, K. *J. Am. Chem. Soc.* **2007**, *129*, 1520. (c) Kunzelman, J.; Kinami, M.; Crenshaw, B. R.; Protasiewicz, J. D.; Weder, C. *Adv. Mater.* **2008**, *20*, 119. (d) Kozhevnikov, V. N.; Donnio, B.; Bruce, D. W. *Angew. Chem., Int. Ed.* **2008**, *47*, 6286. (e) Ito, H.; Saito, T.; Oshima, N.; Kitamura, N.; Ishizaka, S.; Hinatsu, Y.; Wakeshima, M.; Kato, M.; Tsuge, K.; Sawamura, M. *J. Am. Chem. Soc.* **2008**, *130*, 10044. (f) Zhang, G.; Lu, J.; Sabat, M.; Fraser, C. L. *J. Am. Chem. Soc.* **2010**, *132*, 2160. (g) Tsukuda, T.; Kawase, M.; Dairiki, A.; Matsumoto, K.; Tsubomura, T. *Chem. Commun.* **2010**, *46*, 3255. (h) Zhang, G.; Lu, J.; Fraser, C. L. *Inorg. Chem.* **2010**, *49*, DOI: 10.1021/ic902591s.

(9) (a) Mizukami, S.; Houjou, H.; Sugaya, K.; Koyama, E.; Tokuhisa, H.; Sasaki, T.; Kanesato, M. *Chem. Mater.* **2005**, *17*, 50. (b) Yagai, S.; Seki, T.; Karatsu, T.; Kitamura, A.; Würthner, F. *Angew. Chem., Int. Ed.* **2008**, *47*, 3367. (c) Sagara, Y.; Kato, T. *Angew. Chem., Int. Ed.* **2008**, *47*, 5175. (d) Sagara, Y.; Yamane, S.; Mutai, T.; Araki, K.; Kato, T. *Adv. Funct. Mater.* **2009**, *19*, 1869. (e) Chung, J. W.; You, Y.; Huh, H. S.; An, B. K.; Yoon, S. J.; Kim, S. H.; Lee, S. W.; Park, S. Y. *J. Am. Chem. Soc.* **2009**, *131*, 8163. (f) Sagara, Y.; Kato, T. *Nat. Chem.* **2009**, *1*, 605.

(10) (a) An, B. K.; Kwon, S. K.; Jung, S. D.; Park, S. Y. *J. Am. Chem. Soc.* **2002**, *124*, 14410. (b) An, B. K.; Lee, D. S.; Lee, J. S.; Park, Y. S.; Song, H. S.; Park, S. Y. *J. Am. Chem. Soc.* **2004**, *126*, 10232. (c) An, B. K.; Gihm, S. H.; Chung, J. W.; Park, C. R.; Kwon, S. K.; Park, S. Y. *J. Am. Chem. Soc.* **2009**, *131*, 3950.

(11) Oelkrug, D.; Tompert, A.; Gierschner, J.; Egelhaaf, H. J.; Hanack, M.; Hohloch, M.; Steinhuber, E. *J. Phys. Chem. B* **1998**, *102*, 1902.

(12) (a) Lim, S. J.; An, B. K.; Jung, S. D.; Chung, M. A.; Park, S. Y. *Angew. Chem., Int. Ed.* **2004**, *43*, 6346. (b) Lim, S. J.; An, B. K.; Park, S. Y. *Macromolecules* **2005**, *38*, 6236.

(13) An, B. K.; Kwon, S. K.; Park, S. Y. *Bull. Korean Chem. Soc.* **2005**, *26*, 1555.

(14) An, B. K.; Kwon, S. K.; Park, S. Y. *Angew. Chem., Int. Ed.* **2007**, *46*, 1978.

(15) (a) Chung, J. W.; An, B. K.; Park, S. Y. *Chem. Mater.* **2008**, *20*, 6750. (b) Chung, J. W.; Yoon, S. J.; Lim, S. J.; An, B. K.; Park, S. Y. *Angew. Chem., Int. Ed.* **2009**, *48*, 7030.

(16) For general preparation methods of organic nanoparticles, see: (a) Kasai, H.; Nalwa, H. S.; Okada, S.; Oikawa, H.; Nakanish, H. *Handbook of Nanostructured Materials and Nanotechnology*; Academic Press: New York, 2000; Vol. 5, Chapter 8, 433−473. (b) Horn, D.; Rieger, J. *Angew. Chem., Int. Ed.* **2001**, *40*, 4330.

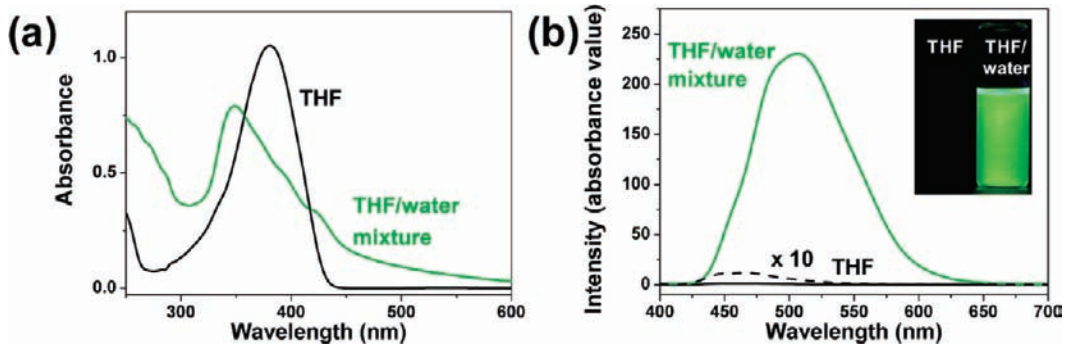

Figure 1. (a) UV−visible absorption spectra of DBDCS in THF solution ($c = 2 \times 10^{-5}$ mol L^{-1}, black line) and DBDCS nanoparticles in THF/water mixture ($c = 2 \times 10^{-5}$ mol L^{-1}, green line). (b) PL spectra of DBDCS in THF solution (black line) and DBDCS nanoparticles in THF/water mixture (green line). Insets show the fluorescence images of DBDCS in THF solution and DBDCS nanoparticles in THF/water mixture under 365 nm UV light.

were recorded on a Shimazu, UV-1650 PC spectrometer. Photoluminescence spectra were obtained using a Shimazu, RF 5301 PC spectrometer. The relative fluorescence quantum yield was measured using 9,10-diphenylanthracence (DPA) in benzene as a standard reference (1×10^{-4} mol L^{-1}, $\Phi_f = 83\%$). Time-resolved fluorescence lifetime experiments were performed by the time-correlated single-photon-counting (TCSPC) technique. As an excitation light source, we used a Ti:sapphire laser (Mai Tai BB, Spectra-Physics) which provides a repetition rate of 800 kHz with ~100 fs pulses generated by a homemade pulse-picker. The output pulse of the laser was frequency-doubled by a 1 mm thickness of a second harmonic crystal (β-barium borate, BBO, CASIX). The fluorescence was collected by a microchannel plate photomultiplier (MCP-PMT, Hamamatsu, R3809U-51) with a thermoelectric cooler (Hamamatsu, C4878) connected to a TCSPC board (Becker and Hickel SPC-130). The overall instrumental response function was about 25 ps (the full width at half-maximum (fwhm)). A vertically polarized pump pulse by a Glan-laser polarizer was irradiated to samples, and a sheet polarizer, set at an angle complementary to the magic angle (54.7°), was placed in the fluorescence collection path to obtain polarization-independent fluorescence decays. The femtosecond time-resolved transient absorption (TA) spectrometer was pumped by a Ti:sapphire regenerative amplifier system (Quantronix, Integra-C) operating at 1 kHz repetition rate and an optical detection system. The frequency doubled 400 nm pulses had a pulse width of ~100 fs and an average power of 1 mW which were used as pump pulses. White light continuum (WLC) probe pulses were generated using a sapphire window (2 mm of thickness) by focusing of small portion of the fundamental 800 nm pulses. The time delay between pump and probe beams was carefully controlled by making the pump beam travel along a variable optical delay (Newport, ILS250). Intensities of the spectrally dispersed WLC probe pulses are monitored by miniature spectrograph (OceanOptics, USB2000+). To obtain the time-resolved transient absorption difference signal (ΔA) at a specific time, the pump pulses were chopped at 25 Hz and absorption spectra intensities were saved alternately with or without pump pulse. Typically, 6000 pulses excite samples to obtain the TA spectra at a particular delay time. The polarization angle between pump and probe beam was set at the magic angle (54.7°) in order to prevent polarization-dependent signals. Cross-correlation fwhm in pump−probe experiments was less than 200 fs and chirp of WLC probe pulses was measured to be 800 fs in the 400−800 nm region. To minimize chirp, all reflection optics in probe beam path and 2 mm path length of quartz cell were used. The three-dimensional data sets of ΔA versus time and wavelength were subjected to singular value decomposition and global fitting to obtain the kinetic time constants and their associated spectra using Surface Xplorer software.

2.5. Quantum Chemical Calculations. Single-molecule calculations in the gas phase were performed at the density functional theory (DFT) level of theory with the Gaussian 03 software.[17] Herein, the ground-state geometry was fully optimized using the B3LYP functional and 6-31+G** basis set. The dipole moment was calculated on the basis of the molecular geometry from single-crystal X-ray analysis. The transition dipole moment was calculated on the basis of the molecular geometry from single-crystal X-ray analysis at the (time-dependent) DFT B3LYP level, using the 6-31+G** basis set. For a first qualitative picture of the excitonic interactions in the system, exciton splitting calculation was performed by a supramolecular approach on a coplanar molecular dimer pair, using ZINDO/S (Zerner's spectroscopic parametrization for intermediate neglect of differential overlap for spectroscopy) method, taking into account full single configuration interaction (SCI) over the occupied- and unoccupied-types of molecular orbitals (MOs).

3. Results

Like structurally similar compounds,[10−15] DBDCS exhibited intense solid-state fluorescence due to the characteristic AIEE process. To easily examine the AIEE process of DBDCS free from artificial effects induced by optically thick samples typically observed for deposited films or powders and also to conveniently measure solid-state fluorescence quantum yields,[11,18] DBDCS nanoparticle suspensions were used. The nanoparticles were prepared by a simple precipitation method, which generates stable suspensions without surfactants by (rather kinetically controlled) spontaneous self-assembly. Field emission scanning electron microscopy (FE-SEM) of nanoparticles which were deposited on a substrate revealed small spheres with a mean diameter of 20−30 nm (see Figure S2 in SI). Parts a and b of Figure 1 show the absorption and emission spectra of DBDCS in THF solution[19] and its nanoparticle suspension (THF/water mixture), respectively. DBDCS exhibits a drastic change of fluorescence intensity from the nonfluorescent THF solution (quantum yield $\Phi_F = 2.6 \times 10^{-3}$) to the strongly fluorescent nanoparticle suspension ($\Phi_F = 0.62$) as demonstrated in the inset photograph of Figure 1b. The fluorescence enhancement upon aggregation thus spans 2 orders of magnitude. At the same time, the fluorescence lifetime τ_F increases from 4.2 ps in solution to 11.9 ns in the nanoparticle suspension (*vide infra*). In the absorption spectra, the peak maximum of the nanoparticle suspension is blue-shifted from 381 to 349 nm with respect to

(17) Frisch, M. J.; et al. *Gaussian 03*; Gaussian Inc.: Wallingford, CT, 2004.
(18) Gierschner, J. *PhD Dissertation*, 2000, Verlag Köhler: Tübingen, ISBN: 3-932694-76-7.
(19) DBDCS solutions show very similar absorption and emission spectra in a series of solvents with a broad range of polarity. The solvent polarity independence in the absorption and emission maxima of DBDCS solution is summarized in Figure S3 in SI.

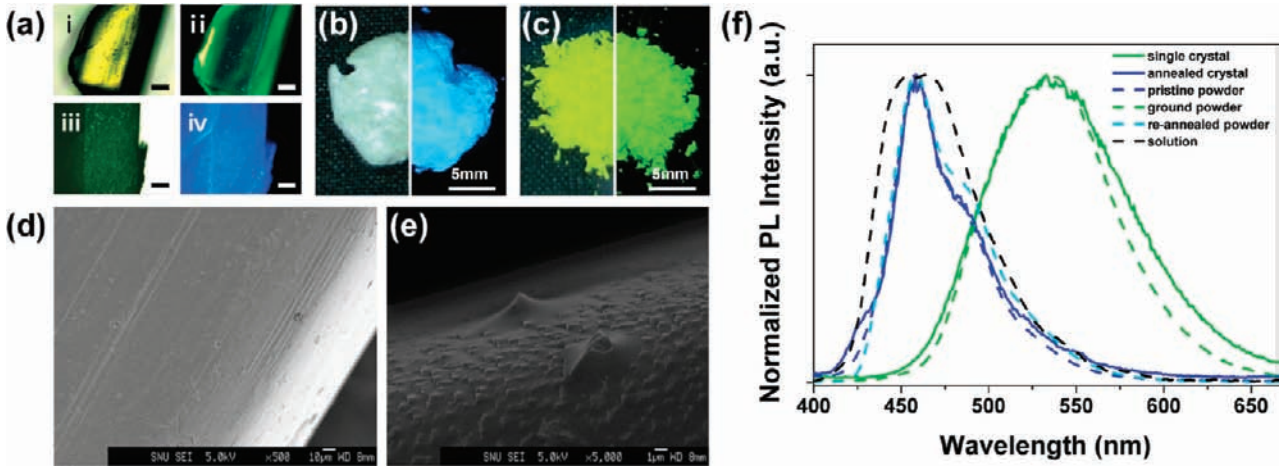

Figure 2. (a) Photo of a single crystal: before annealing, under room light (i), and UV light (ii), and after annealing, under room light (iii), and UV light (iv) (scale bar = 0.2 mm). (b) Photo of the pristine powder under room (left) and UV light (right). (c) Photo of the ground powder under room light (left) and UV light (right). (d) SEM image of the surface morphology of DBDCS single crystal. (e) SEM images of the surface morphology of DBDCS annealed crystal. (f) Normalized PL spectra of DBDCS single crystal (green solid line), annealed crystal (blue solid line), pristine powder (blue dashed line), ground powder (green dashed line), reannealed powder (sky-blue dashed line), solution (black dashed line).

solution, and shows a pronounced asymmetric band shape (note that the excitation PL spectrum of the nanoparticle suspension is almost identical to the absorption spectrum of it, see Figure S4 in SI). Both observations can be attributed to H-type aggregation,[2,20] which is consistent with a substantial decrease of the rate constant $k_F = \Phi_F/\tau_F$ from 6.2×10^8 s^{-1} in solution to 5.2×10^7 s^{-1} in the nanoparticles. The observed H-type aggregation in DBDCS is quite different from previous reports of other cyano stilbene derivatives.[10] The shape of the strongly red-shifted, unstructured emission spectrum of the DBDCS nanoparticle suspension, on the other hand, is reminiscent of excimer emission.[2]

Figure 2a shows the images of DBDCS single crystals as grown from ethyl acetate solution. As prepared, they are yellow in color and emit green light (λ_{max} = 533 nm) under UV illumination (Figure 2f), which is to be called the **G**-phase of DBDCS crystal. Heating the sample to 125 °C for an hour, however, changes the color to pale whitish green and the emission to blue (**B**-phase, 458 nm), while the crystal appearance changes from transparent to opaque (Figure 2, a and f). The crystal surface after annealing, as investigated by FE-SEM, was rough and showed sheetlike regular projections and cracks, indicating a rearrangement of the molecules in the crystal lattice (Figure 2, d and e). In fact, this crystalline-state transition with characteristic fluorescence change upon 125 °C annealing is associated with the first-order endothermic peak in the differential scanning calorimetry (DSC) thermogram (Figure 3a).

Figure 4 shows the molecular packing structures of the **G**-phase DBDCS single crystal (space group $P\bar{1}$, one molecule per unit cell) in different perspectives as determined by single-crystal X-ray analysis (see Table S1 and Figure S1 in SI). Most uniquely, DBDCS crystallizes to form the planar 'molecular sheets' assisted by the multiple C−H···N and C−H···O hydrogen bonds combined with the appropriate length of alkyl substituents (Figure 4c and Figure S5 in SI). It is shown that the molecular sheets in this **G**-phase crystal are arranged in slip-stacks along the long molecular axis with a pitch angle of 26.6°, whereas only a very small slip along the short axis is observed (corresponding to a roll angle of 83.3°), as shown in Figure 4,

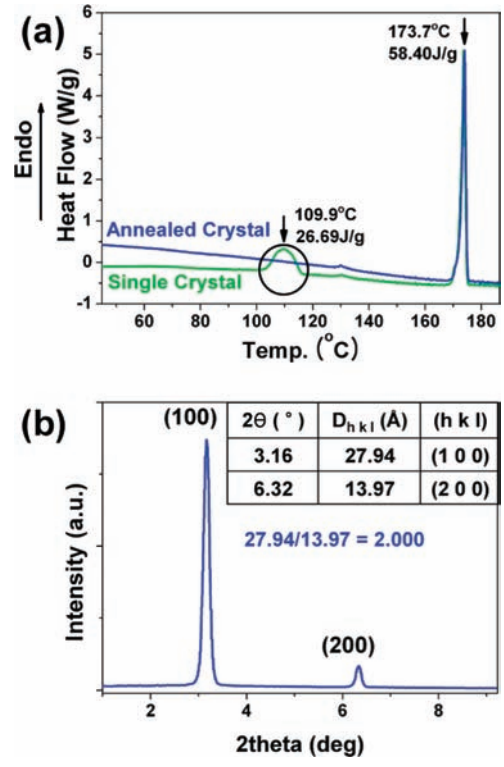

Figure 3. (a) DSC trace (first heating) of single crystal (green line) and annealed crystal (blue line). (b) SAXS pattern of annealed DBDCS crystal (inset: *d*-spacing of the reflection peaks, Miller indices).

a and b. The interlayer distance between the adjacent molecular sheets is 3.7 Å, consistent with other $\pi-\pi$ stacking distances reported earlier for substituted DSBs.[2] The driving force for this specific slip-stack formation is the antiparallel coupling between the local dipoles[21,22] in adjacent molecular sheets (see Scheme 2 for the coupling scheme, and Figure 4a and Figure S6b in SI for the crystallographic data). Since the outer phenyl rings are electron-rich with butoxy-substituents while the central

(20) Kasha, M.; Rawls, H. R.; El-Bayoumi, M. A. *Pure Appl. Chem.* **1965**, *11*, 371.

(21) (a) Cacelli, I.; Feretti, A.; Girlanda, M.; Macucci, M. *Chem. Phys.* **2006**, *320*, 84. (b) Haino, T.; Tanaka, M.; Fukazawa, Y. *Chem. Commun.* **2008**, 468.

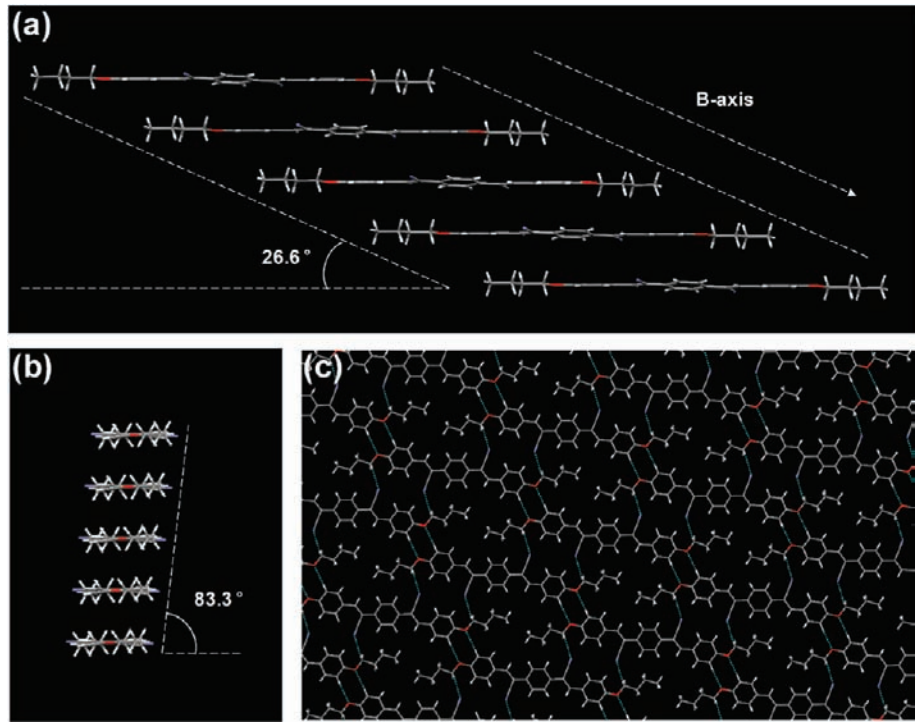

Figure 4. G-phase DBDCS molecules in the crystal structure: (a) Side view and illustration of pitch angle. (b) Front view and illustration of roll angle. (c) Top view and illustration of hydrogen-bonded molecular sheet.

Scheme 2. Illustration of Two Different Modes of Slip-Stacking in DBDCS Molecular Sheets, Dictated by Different Ways of Antiparallel/Head-to-Tail Coupling of Local Dipoles

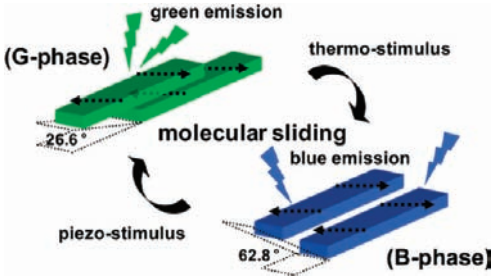

phenyl ring is electron-poor with cyano groups, DBDCS is a D−A−D molecule comprising two local dipoles (Scheme 1) which add to a zero net dipole moment. As illustrated in Figure 4a, antiparallel dipole coupling places the central 'A' ring of the upper sheet just above the 'D' ring of the lower sheet, bringing about efficient excitonic and excimeric coupling between DBDCS molecules (*vide infra*).

Thermal annealing of the **G**-phase crystal to the **B**-phase must accompany specific stacking changes, which unfortunately could not be monitored by single crystal X-ray analysis due to the poor crystal quality of **B**-phase DBDCS as mentioned above. Instead, the small-angle X-ray scattering (SAXS) pattern of the blue-emitting crystal could be measured to show (100) and (200) reflection peaks of lamellar structure (Figure 3b). Comparing the *d*-spacing (27.9 Å) with the molecular van der Waals length of 31.4 Å, we could infer a different slip-stack featuring an angle of 62.8°; however, the exact pitch/roll angles are unknown. For reasons to be discussed below (*vide infra*), we suggest that the principal slip direction of the molecular sheets is along the shorter axis of DBDCS molecule to effectively offset the aromatic rings and establishing efficient head-to-tail coupling of the local dipoles in adjacent molecular sheets (see Scheme 2 for the coupling situation).

Blue-emitting DBDCS powder could alternatively be prepared by recrystallization from hot ethanol solutions as pale whitish sheet-like crystallites, as shown in Figure 2b. Interestingly, when grinding the blue powder in a mortar or rubbing it with a spatula, it was observed that the fluorescence color changed immediately to green (Figure 2c). This piezochromic transition[8,9] thus represents the reversal of the annealing process and is likely to be driven by the stacking mode change as well. As a matter of fact, the mechanically ground green-emitting powder of DBDCS returns to the original blue-emitting one by brief thermal annealing at 125 °C for 5 min (see Figure S8 in SI). It is important to note that the emission spectra of the reversible piezochromism process exactly matches those of the **B**- and **G**-phases of the single crystal, as shown in Figure 2f and extensively summarized in Table 1. Namely, the structured blue emission spectra of both the pristine and the reannealed powders are centered at 458 nm, i.e. the same as the **B**-phase of the annealed crystal, and the unstructured green emission spectrum of the ground powder, centered at 536 nm, corresponds to the spectrum of the **G**-phase single crystal. Concomitantly, the SAXS pattern of blue-emitting powder shows the same *d*-spacing as that of the annealed crystal (**B**-phase) (see Figure S7 and Table S2 in SI). The mechanically ground green-emitting powder gave a *d*-spacing of 21.9 Å and thus a slip angle of 44.2°. However it should be noted that the piezo-process is not a complete conversion process since the shear force applies unevenly to the bulk pristine powder. The remaining peaks corresponding to the pristine powder are always included in

(22) (a) Gill, R. E.; vanHutten, P. F.; Meetsma, A.; Hadziioannou, G. *Chem. Mater.* **1996**, *8*, 1341. (b) Kishikawa, K.; Furusawa, S.; Yamaki, T.; Kohmoto, S.; Yamamoto, M.; Yamaguchi, K. *J. Am. Chem. Soc.* **2002**, *124*, 1597. (c) Yasuda, T.; Imase, T.; Nakamura, Y.; Yamamoto, T. *Macromolecules* **2005**, *38*, 4687.

Table 1. Spectroscopic and Structural Data of the Observed Phases for the Different Systems Prepared in This Work

	B-phase				**G**-phase			
		λ_{abs} (nm)	λ_{em} (nm)	slip angle (deg)		λ_{abs} (nm)	λ_{em} (nm)	slip angle (deg)
nanoparticles	—				pristine[a]	349	507	—
single crystal	annealed	—	458	62.8	pristine	—	533	pitch: 26.6 roll: 83.3
powder	pristine	—	458	62.8	pressure	—	536	44.2
	reannealed	—	458	62.8				
VD film	$T_S = 100$ °C	303	457	60.4	$T_S = 25$ °C	340	538	46.0
PMMA film	annealed	302	457	—	pristine[a]	339	510	—
					pressure	361	523	—
					vapor[a]	339	510	—

[a] Probably (slightly) different crystal structure from **G**-phase with rather loose crystalline order due to the spherical particle shape.

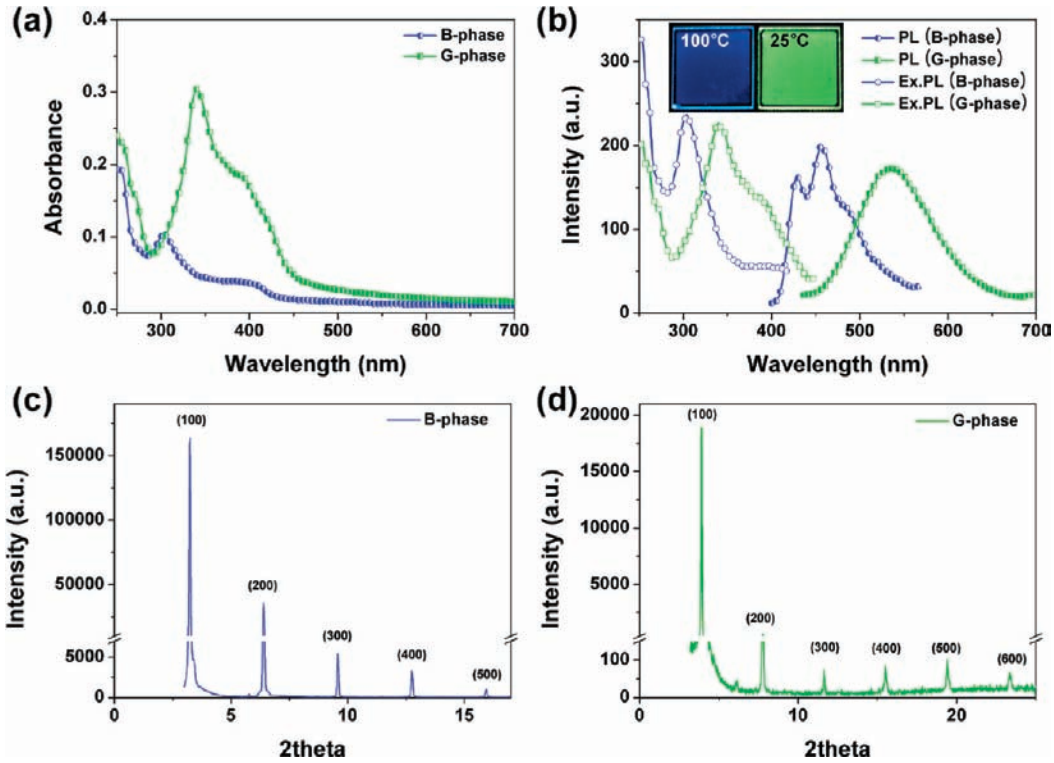

Figure 5. DBDCS vacuum-deposited thin film with substrate temperature of 100 °C (**B**-phase VD film, blue line) and 25 °C (**G**-phase VD film, green line): (a) UV−visible absorption spectra (b) PL spectra (filled symbols) and excitation PL spectra (open symbols). Insets show the fluorescence images of DBDCS thin film with substrate temperature of 100 and 25 °C under 365 nm UV light. (c) XRD pattern of DBDCS thin film with substrate temperature of 100 °C. (d) XRD pattern of DBDCS thin film with substrate temperature of 25 °C.

the SAXS patterns of the ground powder. However, reannealing of the ground green-emitting powder completely recovers the initial SAXS pattern, which confirms the same nature of blue emission in the pristine and reannealed powder. Thus, in all, we could identify two distinctively different phases—'green' (**G**) and 'blue' (**B**)—in both single crystal and powders, which can be reversibly switched, from **G** to **B** by thermal annealing and from **B** to **G** by pressure through a specific phase transition induced by two-directional shear-sliding capability of the molecular sheets (see Table 1 for details).

G- and **B**-phases can also be observed in thin films (thickness of 50 nm) prepared by vacuum deposition (VD) on quartz substrates, where the phase formation depends sensitively on the substrate temperature T_S during deposition. The **B**-phase was obtained at $T_S = 100$ °C, with a similar emission spectrum (Figure 5b) as compared to the annealed powder and single crystal spectra discussed above. Accordingly, the XRD pattern of the **B**-phase VD film (Figure 5c) (here of a rather thick sample, i.e. suitable for X-ray investigation) showed similar *d*-spacing (27.3 Å) and slip angle (60.4°) to those of the annealed powder. On the other hand, the **G**-phase VD film was obtained at $T_S = 25$ °C with the emission spectrum (Figure 5b) again coinciding with the ground powder and the single crystal spectrum (see Figure 2). XRD pattern of **G**-phase VD film (Figure 5d) showed similar *d*-spacing (22.6 Å) and slip angle (46.0°) to those of the ground powder sample as expected (see Table 1).

Different from the optically thick samples (crystals, powder) described above, the absorption spectra of thin VD films could be conveniently recorded. As already described for the nanoparticle suspension, the **G**-phase of the VD film also shows H-type aggregation in the absorption spectrum,[2,20] shifting the maximum from 381 nm in solution to 340 nm in film (Figure 5a). In the **B**-phase, H-aggregation is obviously stronger, with the absorption maximum observed at 303 nm. The photoluminescence excitation (PLE) spectra in Figure 5b confirm the conclusions made from the absorption spectra. We want to stress at this point that the measurements on thicker samples, e.g. thick

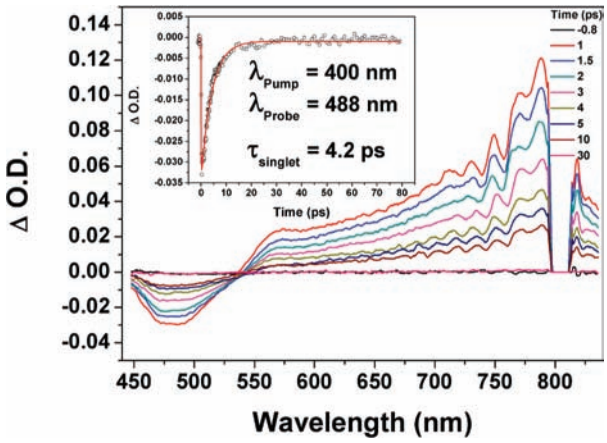

Figure 6. Femtosecond transient absorption spectra of DBDCS under 400 nm excitation in THF solution. Inset shows a decay profile and fitting line at 488 nm.

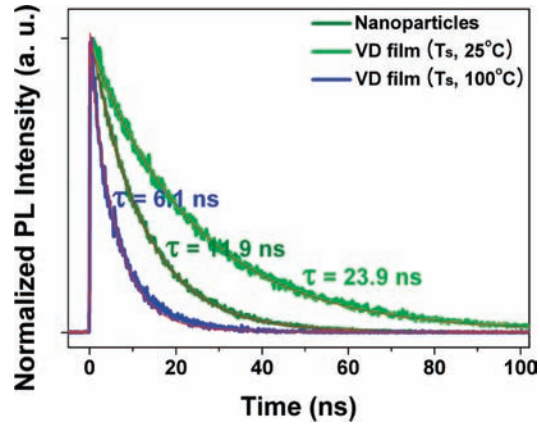

Figure 7. Fluorescence decay profiles of DBDCS nanoparticles in THF/water mixture (dark green line), **G**-phase VD film (green line), **B**-phase VD film (blue line) under 400 nm excitation. Red lines are the best fitting curves.

VD and spin-coated films or smeared powders are highly problematic to make conclusive judgments on H- or J-aggregation since the large optical thickness often leads to saturation phenomena, which might mask the intrinsic optical properties in both absorption and PLE spectra to generate artifact in their spectral shape.[11,18] In this regard, optically thin samples (e.g., thin VD films, or dilute nanoparticle suspensions) are crucial for a correct assignment.

To explore the singlet excited state dynamics of DBDCS in THF solution, nanoparticle suspension, and **G**/**B**-phase VD films, we have carried out the femtosecond transient absorption and time-correlated single photon counting (TCSPC) measurements by 400 nm femtosecond laser excitation. First, the transient absorption spectra of DBDCS in THF solution exhibit stimulated emission (SE) corresponding to the steady state emission band and broad excited-state absorption (ESA) signals in the range of 550−800 nm. And the decay profile at SE (488 nm) band can be fitted to a single exponential function with the time constant of 4.2 ps (Figure 6). This ultrafast excited state dynamics of DBDCS in THF solution is well correlated with the nonfluorescence behavior. On the other hand, the emission lifetimes of DBDCS nanoparticle suspension (11.9 ns), **G**-phase VD film (23.9 ns), and **B**-phase VD film (6.1 ns) are almost several thousand times longer than that of solution (Figure 7).

4. Discussion

The detailed structural information on the observed reversible **G**/**B** phase transition of DBDCS and the comprehensive optical and photophysical characterization allow for a unique insight into the structure−property relationships in π-conjugated organic materials, which will be elucidated in the following with the help of molecular modeling.

In solution, the molecule is practically nonfluorescent, which can be in principle attributed to a small radiative or a large nonradiative rate constant. The radiative rate constant ($k_F = \Phi_F/\tau_F$) in solution is high, $k_F = 6.2 \times 10^8\ s^{-1}$, which is similar to the parent highly fluorescent distyrylbenzene (DSB) in solution and to other (non)fluorescent substituted DSB systems.[23] It also agrees well with the expectation according to the Strickler−Berg formula for the strongly allowed $S_0 \rightarrow S_1$ optical transition in DBDCS, which is responsible for the emission process,[23] and thus cannot be the source for the low Φ_F. Hence, the latter is clearly associated with the nonradiative decay channel, with an estimated rate constant of $k_{nr} = (1 - \Phi_F)/\tau_F = 2.4 \times 10^{11}\ s^{-1}$, which is mainly a consequence of the nonplanarity of DBDCS in both the ground (S_0) and excited state (S_1), which enables torsional-induced nonradiative deactivation as discussed earlier.[11] Indeed, the optimized ground state of DBDCS at the DFT level calculation shows a strong twisting of the outer phenyl rings with dihedral torsional angles of 28.0° and 4.9° (for notation see Scheme 1 and Figure S9a [SI]), in agreement with the previous investigations.[11,24]

Our X-ray analysis in the solid state reveals a substantial planarization in the solid state. The core phenyl ring is much less twisted to the outer phenyl ring with both dihedral torsional angles of 5.6° (Scheme 1 and Figure S9b [SI]). Such pronounced planarization in the crystalline state is not always observed for CN-substitution in the vinylene unit,[11,24] where the dihedral torsion angles became larger with additional substituents in the central phenyl ring. In our case, the planarity is now promoted by the presence of multiple hydrogen-bonds in the DBDCS crystal (see Figure 4c), which gives a substantial planarization and thus effectively locks their conformations in the crystal lattice. This aggregation-induced planarization generates the AIEE phenomenon of DBDCS, which significantly reduces the nonradiative deactivation pathways compared to solution. With $\Phi_f = 0.62$ and $\tau_F = 11.9$ ns, the latter is now $k_{nr} = 3.2 \times 10^7\ s^{-1}$, thus 4 orders of magnitudes smaller than that in solution.

The substantial reduction of the radiative rate constant ($k_F = 5.2 \times 10^7\ s^{-1}$) in the nanoparticle suspension by 1 order of magnitude compared to the solution ($k_{F,solution} = 6.2 \times 10^8\ s^{-1}$) can be unambiguously described as the H-type aggregation due to the excitonic coupling between the transition dipoles of adjacent molecules, which leads to a blue shift in the absorption and forbidden (or only slightly allowed) lowest excited state, concomitantly a small oscillator strength and thus a small k_F.

(23) (a) Oelkrug, D.; Tompert, A.; Egelhaaf, H.; Hanack, M.; Steinhuber, E.; Hohloch, M.; Meier, H.; Stalmach, U. *Synth. Met.* **1996**, *83*, 231. (b) Gierschner, J.; Oelkrug, D.; Nalwa, H. *Encyclopedia of Nanoscience and Nanotechnology*; American Scientific Publishers: Stevenson Ranch, CA, 2004; Vol. 8, pp 219−238.

(24) (a) Souza, M. M.; Rumbles, G.; Gould, I. R.; Amer, H.; Samuel, I. D. W.; Moratti, S. C.; Holmes, A. B. *Synth. Met.* **2000**, *111*, 539. (b) Lange, F.; Hohnholz, D.; Leuze, M.; Ryu, H.; Hohloch, M.; Freudenmann, R.; Hanack, M. *Synth. Met.* **1999**, *101*, 652.

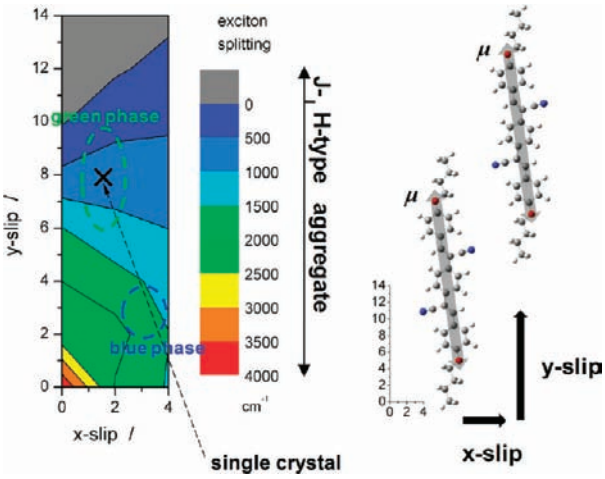

Figure 8. Color contour map of calculated exciton splittings for a dimer pair at a different displacements *x*, *y* (in Å); the separation in *z* amounts 3.7 Å. A slip of 4 Å (**14**) corresponds to a translation by half a molecular length in *x* (*y*).

The situation is similar in the **G**-phase crystal, whose spectral features are akin to those of the nanoparticle suspension. In addition, the emission lifetime is quite long (23.9 ns) (see Figure 7), and clear H-aggregation behavior is observed in the absorption spectrum (Figure 5b). The overall exciton splitting can be estimated from the energy difference between the absorption maximum (340 nm) and the onset of absorption (410 nm),[25] which amounts to 5000 cm^{-1}. A simple dimer calculation with the single crystal X-ray structure gives an excitonic splitting of 800 cm^{-1} (see Figure 8), which should be reasonable, keeping in mind the three-dimensional character of the crystal and the expected breakdown of the nearest-neighbor approximation.[25] The small displacement along the short axis (*x*) of adjacent molecules in the **G**-phase leads to a substantial overlap of the π-systems and, thus considerable excited state delocalization. The latter allows for efficient vibronic coupling of interchromophore breathing modes, which is responsible for the significantly red-shifted and unstructured 'excimer-like' emission.[2,26,27]

Upon thermal treatment, the metastable **G**-phase transforms into the thermodynamically favored **B**-phase, aided by energy efficient slip along the molecular sheets. Both the absorption and emission spectra point to a pronounced different coupling situation; the substantially larger hypsochromic shift of the absorption spectrum suggests a stronger coupling with an exciton splitting of 8600 cm^{-1} as estimated from the absorption spectra. On the other hand, the emission spectrum of the **B**-phase gains vibronic structure and shows a pronounced hypsochromic shift (see Figure 5b), indicating a loss of excited state delocalization between adjacent molecules by a substantial reduction of $\pi-\pi$ overlap. As a result, the emission lifetime becomes also shorter (6.1 ns) than that of the G-phase (Figure 7). In order to reduce such overlap, the slip in the **B**-phase must be essentially along the short *x*-axis, and not like in the **G**-phase along *y*. Indeed, as seen in Figure 8, an *x*-slip leads to a substantial increase of

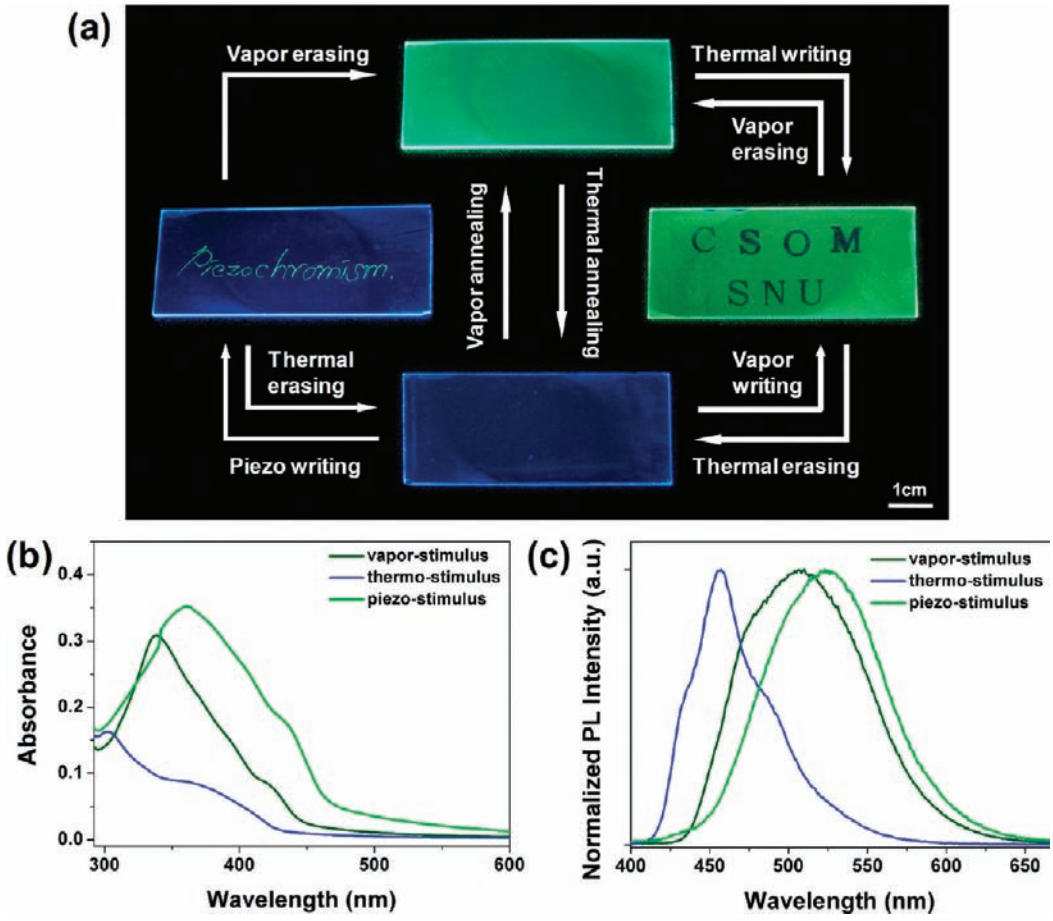

Figure 9. DBDCS/PMMA film: (a) Photos of the luminescence writing/erasing cycle. (b) UV−visible absorption spectra under vapor- (dark green line), thermo- (blue line), piezo- (green line) stimulus. (c) PL spectra under vapor- (dark green line), thermo- (blue line), piezo- (green line) stimulus.

excitonic coupling roughly by a factor of 2, in a good agreement with the experimental result.

At this point, we stress that the phase transition observed here is a quite unique example to study separately exciton and excimer coupling in molecular crystals; while the **G**-phase shows rather weak excitonic coupling, excimer formation is favored by pronounced overlap of the π-systems. In the **B**-phase, excimer formation is diminished, while excitonic interaction substantially increases. The driving force for the phase transition is clearly provided by the local dipoles as introduced through the cyano group. While in the metastable **G**-phase antiparallel coupling of the local dipoles kinetically stabilizes the structure, a smooth slip of the molecular sheets with a very low activation barrier leads to the formation of the **B**-phase with the energetically favored formation of a head-to-tail arrangement of the local dipoles (see Scheme 2).

5. Multistimuli Device Demonstrator

As a practical fast-responding demonstrator for multistimuli luminescence tuning, we prepared a green-emitting (**G**-phase) composite film of DBDCS in PMMA (20 wt %) by spin coating on glass. The surface morphology of the film indicates a phase separation with small grains of about 10 nm size (see Figure S11 in SI). When thermal stimulus (125 °C for 10 s with hot letter stamp) was applied, the green fluorescence changed to blue (Figure 9), in accordance with the **G**- to **B**-phase transition. The thermally annealed **B**-phase film showed high pressure-sensitivity, changing the emission color immediately to green even with a very small shear force, thus allowing for sensitive piezo-writing as shown in Figure 9. Upon exposing the whole films to the organic vapor (CH_2Cl_2 for 30 s), we were able to erase this piezo-writing, changing the entire emission color to green (Figure 9a). The possibility of vapor adsorption in altering the fluorescence color is excluded by vacuum treatment after vapor exposure. In any case, it should be noted that **G**-phase induced by the exposure to vapor is basically same with but slightly different from the **G**-phase induced by shear force, as evident from the comparison of the emission spectra in Figure 9c as well as the absorption spectra in Figure 9b. This implies that vapor exposure also promotes an alternation of the slip-stacking, although to a somewhat different degree compared to the case of pressure application.

Under all these conditions, a reproducible and fully reversible two-color fluorescence writing/erasing process was achieved and both emission colors of blue and green were found to be persistent over one year of observation under ambient conditions. In this way, a rewritable fluorescent optical recording media was newly demonstrated.

6. Conclusion

We have synthesized and fully characterized a novel multistimuli luminescence switching material (DBDCS) with highly enhanced fluorescence emission in the solid state. DBDCS uniquely forms highly fluorescent ($\Phi_F = 0.62$) 'molecular sheets' assisted by the multiple C−H···N and C−H···O hydrogen-bonds with stacking and shear-sliding capabilities via external stimuli (temperature, pressure, solvent vapor). On the basis of structural, optical, photophysical, and computational studies, we identified two different phases, i.e. the metastable green-emitting **G**-phase and the thermodynamically stable blue-emitting **B**-phase, and elucidated the phase transition pathways as well as their spectroscopic implications. In the **G**-phase, antiparallel coupling of the local dipoles kinetically stabilizes a structure with rather moderate excitonic coupling, but efficient excimer formation. Upon annealing, a smooth slip of the molecular sheets with a low activation barrier forms the **B**-phase with a head-to-tail arrangement of the local dipoles. Here the excimer formation is diminished, while excitonic interaction substantially increases. It was found that the application of pressure to the **B**-phase crystal could restore the original **G**-phase. With this concept at hand, we have successfully demonstrated rewritable fluorescent optical recording media which showed fast-responding and reversible multistimuli luminescence switching.

Acknowledgment. This work was supported by the Basic Science Research Program through the National Research Foundation of Korea (NRF) funded by the Ministry of Education, Science, and Technology (CRI; RIAMIAM0209(0417-20090011)). J.G. is a Ramón y Cajal research fellow of the Spanish Ministry for Science and Innovation. The work at Yonsei University was supported by the Star Faculty and World Class University (R32-2008-000-10217-0) Programs from the Ministry of Education, Science, and Technology (MEST) of Korea and the AFSOR/AOARD Grant (FA2386-09-1-4092).

Supporting Information Available: Complete ref 17, synthesis, characterization, crystallographic data (CIF file - CCDC 778284), experimental details, and a movie of the piezo-writing process. This material is available free of charge via the Internet at http://pubs.acs.org.

JA1044665

(25) Gierschner, J.; Huang, Y. S.; Van Averbeke, B.; Cornil, J.; Friend, R. H.; Beljonne, D. *J. Chem. Phys.* **2009**, *130*, 044105.
(26) Hayer, A.; de Halleux, V.; Köhler, A.; El-Garoughy, A.; Meijer, E. W.; Barberá, J.; Tant, J.; Levin, J.; Lehmann, M.; Gierschner, J.; Cornil, J.; Geerts, Y. H. *J. Phys. Chem. B* **2006**, *110*, 7653.
(27) Gierschner, J.; Mack, H. G.; Oelkrug, D.; Waldner, I.; Rau, H. *J. Phys. Chem. A* **2004**, *108*, 257.